Reorganization energy upon charging a single molecule on an insulator measured by atomic force microscopy

Shadi Fatayer,[1,*] Bruno Schuler,[1,†] Wolfram Steurer,[1] Ivan Scivetti,[2,‡] Jascha Repp,[3] Leo Gross,[1] Mats Persson,[2,4] and Gerhard Meyer[1]

[1]*IBM Research – Zurich, Säumerstrasse 4, 8803 Rüschlikon, Switzerland*

[2]*Surface Science Research Centre, Department of Chemistry, University of Liverpool, Liverpool, L693BX, United Kingdom*

[3]*Institute of Experimental and Applied Physics, University of Regensburg, 93053 Regensburg, Germany*

[4]*Department of Applied Physics, Chalmers University of Technology, SE 41296, Göteborg, Sweden*

(Dated: January 25, 2018)

Intermolecular single-electron transfer on electrically insulating films is a key process in molecular electronics [1–4] and an important example of a redox reaction [5, 6]. Electron-transfer rates in molecular systems depend on a few fundamental parameters, such as inter-adsorbate distance, temperature and in particular, the Marcus reorganization energy [7]. This crucial parameter is the energy gain resulting from the distortion of the equilibrium nuclear geometry in the molecule and its environment upon charging [8, 9]. The substrate, especially ionic films [10], can have an important influence on the reorganization energy [11, 12]. Reorganization energies are measured in electrochemistry [13] as well as with optical [14, 15] and photoemission spectroscopies [16, 17], but not at the single molecule limit nor on insulating surfaces. Atomic force microscopy, with single-charge sensitivity [18–22], atomic-scale spatial resolution [20] and operable on insulating films overcomes these challenges. Here, we investigate redox reactions of single naphthalocyanine molecules on multilayered NaCl films. Employing the atomic force microscope as an ultra-low current meter, allows us to measure the differential conductance related to transitions between two charge-states in both directions. Thereby, the reorganization energy of naphthalocyanine on NaCl is determined as (0.8 ± 0.2) eV, while density functional theory calculations provide the atomistic picture of the nuclear relaxations upon charging. Our approach presents a route to perform tunneling spectroscopy of single adsorbates on insulating substrates and provides insight into single-electron intermolecular transport.

The chemical structure of naphthalocyanine (NPc) and the constant frequency shift Δf image of NPc on NaCl are shown in Fig. 1a. NPc is adsorbed on a 14 monolayer (ML) NaCl film supported by a Cu(111) substrate (see Figure S1) at 5 K. Due to the NaCl film thickness, electron tunneling through the film is quenched and the only possible electron transfer pathway is between tip and NPc, as sketched in Fig. 1b.

We measure the hole reorganization energy E_{reorg} of a single-molecule adsorbed on an insulating film based on a statistical analysis of single-electron transfer measurements between a metallic tip and NPc. . Fig. 1c depicts the atomic force microscopy (AFM) detection of a single electron transfer cycle involving an outer-sphere [13] redox reaction of NPc ($NPc^0 \rightarrow NPc^+ \rightarrow NPc^0$). An electron is detached from the highest occupied molecular or-

bital (HOMO) by sweeping the sample voltage, starting from 0 V, at approximately −2.3 V. This corresponds to an oxidation of NPc^0 ($NPc^0 \rightarrow NPc^+$, denoted as ox^0). The electron transfer from the molecule to the tip is identified as a step in the frequency shift vs. sample voltage ($\Delta f(V)$) spectrum [20]. The horizontal shift of the extrapolated Kelvin probe parabolas (dashed lines) indicates that the molecule becomes positively charged. Subsequently, sweeping from negative voltages back to zero leads to the electron reattachment to NPc^+ from the tip, corresponding to a reduction of NPc^+ ($NPc^+ \rightarrow NPc^0$, denoted as red^+). Interestingly, red^+ occurs at a less negative voltage than ox^0, which results in a hysteretic behavior of the oxidation and reduction cycle.

The observed difference in the oxidation and reduction voltages is an effect of the reorganization energy, which can be understood from the corresponding single electron transfer processes. These processes are the vertical (Franck-Condon) transitions ox^0 (red^+), occurring at fixed equilibrium geometry geo^0 (geo^+) of NPc^0 (NPc^+), as schematically displayed in Fig. 1d. The net energy change for the oxidation and reduction (the sum of the ox^0 and red^+ energy changes) equals the reorganization energy E_{reorg}. E_{reorg} is associated with the relaxations of the nuclear positions, i.e. the relaxation energies λ_+ and λ_0, also called heterogeneous reorganization energies [23].

Therefore, E_{reorg} is given by the energy difference between red^+ and ox^0 energy levels. Both levels can be probed by single electron tunneling at appropriate voltages. By starting with NPc^0 (NPc^+) and varying the sample voltage, the Fermi level of the metal tip aligns with the ox^0 (red^+) energy level and an electron tunnels to (from) the tip, as schematically represented in the electron energy diagram in Fig. 1e. In a free energy picture, the applied bias voltages will shift one specific charge state curve vertically with respect to the other. For the voltages associated with the ox^0 (red^+) energy level, the minimum in free energy of the NPc^0 (NPc^+) configuration intersects with the free energy curve of NPc^+ (NPc^0) and an electron is transferred to (from) the tip from (to) the molecule. Experimentally determining E_{reorg}, then, requires measuring the voltages associated with the red^+ and ox^0 energy levels. However, many repetitions of the charge transfer cycle reveal that the red^+ and ox^0 voltages vary between measurements (indicated as gray shading in Fig. 1c) and therefore requires statistical analysis. These fluctuations occur because each transition reflects only one single tunneling event, being stochastic in nature. In addition, the ox^0 (red^+) levels are significantly broadened due to the strong coupling between an electron and the optical phonons in the

ionic film and the zero-point fluctuations of their phonon coordinates at the low temperature of the experiment [10, 24, 25].

If both the ox^0 and red^+ processes could be observed in a steady-state situation then the corresponding current would already represent an average of the statistical tunneling process as, for example, in the electron detachment measurement of molecules on a bilayer NaCl with scanning tunneling spectroscopy [25]. In this case, the current is proportional to the corresponding transition rate. Here, however, we could not rely on such intrinsic self-averaging, but instead detect individual tunneling events. The transition rate can then be obtained from the average rate over many individual events. This new statistical approach to measure the rate of a specific charge state transition is summarized in Fig. 2 for transitions between NPc^0 and NPc^+. First, the molecule was set to the desired charge state NPc^0 (NPc^+) by applying a voltage significantly above the red^+ (below the ox^0) voltage (see Fig. 1e) and by approaching the tip closely to the molecule at a distance z_{set}, in order to provide a high tunneling rate. The electron transfer was then probed at appropriate values of voltage V_{probe} and tip height z_{probe}. The latter was adjusted such that the charge transfer was detectable within the time-resolution of 0.1 s of our setup. z_{probe} and z_{set} are defined in the Methods section. The charge state was probed for a fixed probe time T of approximately 9 s and changes in the charge state were identified as steps in $\Delta f(t)$. Such a single 'set-probe' measurement is shown for the red^+ transition in Fig. 2a. The statistical variation of the tunneling process was accounted for a record of 80 probe traces in total at a fixed V_{probe} (as shown in Fig. 2b) obtained in four different sets of measurements. After each set of measurements the Δf feedback was enabled before measuring another set. The blue and green areas in the histograms shown in Fig. 2c,d correspond to the averaged residence times in the NPc^0 and NPc^+ state during the probe time T. The fraction r of the total probe time in which the molecule remains in the set charge state, at a certain V_{probe}, is given by

$$r = \frac{A_{set}}{A_{set} + A_{final}} = \frac{\left(1 - e^{-\Gamma T}\right)}{\Gamma T}. \quad (1)$$

Here A_{set} and A_{final} are the areas representing the averaged residence times during the probe time T of the initially set and the final charge states, respectively. These areas are obtained from the Δf histograms of all probe traces and exemplified in Fig. 2c in green and blue, respectively. The tunneling rate Γ is the inverse of τ, the lifetime of the set charge state at probing conditions (derivation details are provided in the Supplemental Information). The

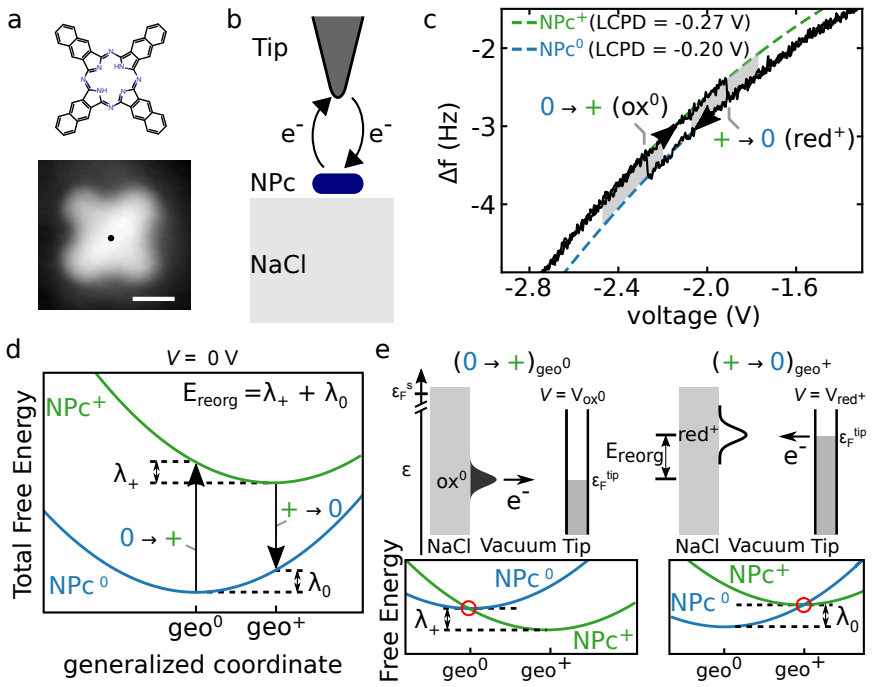

FIG. 1. AFM measurements of naphthalocyanine on a 14 ML NaCl film. **a,** Chemical structure of NPc and AFM constant Δf image (Δf = -1.7 Hz, V = 1 V) of NPc on multilayer NaCl. The black dot indicates the spectrum position in **c**. The scale bar is 10 Å. **b,** Sketch of the experimental arrangement. Due to the thick NaCl film, electron transfer is only possible between tip and NPc, but not between Cu(111) and NPc. **c,** $\Delta f(V)$ spectrum recorded on a NPc molecule. Δf steps indicate an electron detachment from or reattachment to the highest occupied molecular orbital (HOMO). The dashed lines represent Kelvin parabolas of the neutral (NPc^0) and cation (NPc^+) species. Grey areas highlight the observed variation of voltages for electron detachment and reattachment. Note that the spectrum was recorded at a closer distance compared to other measurements in this publication to increase the transfer rate. **d,** Schematic of the total free energy curves for NPc^0 and NPc^+ with respect to the Fermi level of the tip at V = 0 V. The relaxation energy (also called heterogeneous reorganization energy) λ_+ is the energy difference between the energies of geo^0 and geo^+ along the NPc^+ potential energy curve. The relaxation energy λ_0 is the analogous for NPc^0. The hole reorganization energy E_{reorg} is the sum of λ_+ and λ_0. **e,** Electron energy ε diagrams corresponding to the sample voltages of electron detachment from NPc to the tip (ox^0, left) and electron reattachment from the tip to NPc (red^+, right). The difference in electron energies corresponds to the Marcus reorganization energy. In the bottom, the corresponding pictures for the total free energy at the respective sample voltage are depicted.

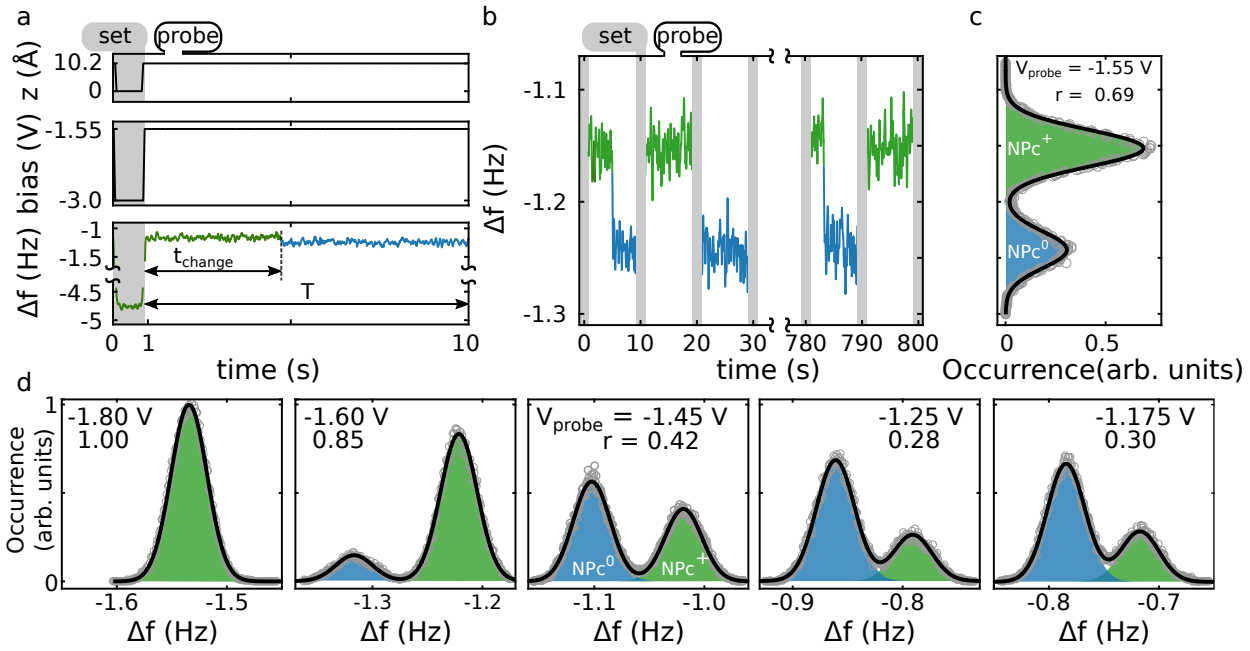

FIG. 2. Single-electron tunnel spectroscopy. **a,** Tip height z, sample voltage and $\Delta f(t)$ spectra for one probe cycle of electron reattachment (red$^+$) to NPc. $\Delta f(t)$ indicates the measured residence time t_{change} in the initial set charge state. z_{probe} is the additional tip-surface distance with respect to the set point value. **b,** First three and last two of eighty measured probe traces $\Delta f(t)$ for $V_{\mathrm{probe}} = -1.55\,\mathrm{V}$. **c,** Histogram of the time integrated Δf of all probe traces measured for $V_{\mathrm{probe}} = -1.55\,\mathrm{V}$. Gaussians are fitted to the peaks. r denotes the fraction of the probe time in which the molecule remains in the set charge state (NPc$^+$, in this case) as obtained from the areas in the histogram (cf. Eq. (1)). **d,** Evolution and saturation of the Δf histograms for different V_{probe}.

evolution of r as a function of V_{probe} for the red$^+$ transition is shown in Fig. 2d. Starting from $r = 1$ at $V_{\mathrm{probe}} = -1.8\,\mathrm{V}$, indicating $\tau \gg T$, r decreases until it reaches a saturation value $r_{\mathrm{sat}} \approx 0.3$ at a greater V_{probe}.

Next we derive the single-electron differential tunneling rate to determine the ox^0 and red$^+$ voltages. For every V_{probe}, the rate Γ can be derived from the experimentally determined $r(V_{\mathrm{probe}})$ (see Eq. (1)). Γ can be interpreted as a single-electron tunneling current when multiplied by the elementary charge e. Consequently, the measured Gaussian-shaped differential conductance in the case of bilayer NaCl insulating films [10] translates to a Gaussian shape of the corresponding $d\Gamma/dV_{\mathrm{probe}}$ in this experiment. Therefore, $\Gamma(V_{\mathrm{probe}})$ is well fitted by an error function. The derivative of this fitting function is analogous to a

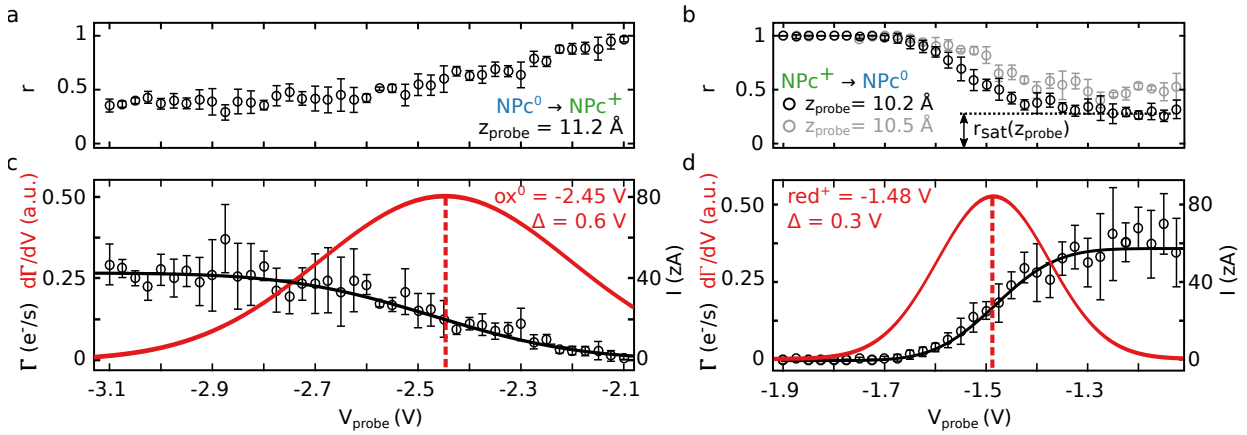

FIG. 3. Analysis of the charge-state transitions as a function of sample probe voltage V_{probe}. **a,c** HOMO — ox^0 ($NPc^0 \rightarrow NPc^+$). **b,d** HOMO — red^+ ($NPc^+ \rightarrow NPc^0$). **a** and **b** display the behavior of r as a function of V_{probe} (the saturation value r_{sat} along with the r results for a different z_{probe} are indicated in **b**). r denotes the fraction of the probe time in which the molecule remains in the set charge state as obtained from the areas in the histogram (cf. Eq. (1)). The error bars are the standard error of the mean r of each individual set of measurements of r. **c** and **d** represent the respective calculated tunneling rate Γ (the analogous value of tunneling current I is displayed in the right axis) along with the fitted error function (black line) and its derivative (red line) representing the respective orbital resonance. The peak positions ox^0 and red^+ (dashed vertical lines) and the full width at half maximum Δ of each peak are indicated in both graphs.

differential conductance, the maximum of which determines the ox^0 and red^+ voltages. In this analysis we assumed that the energy barrier is approximately constant for the voltage window of V_{probe}. The additional broadening due to the tip oscillation amplitude of 6 Å is negligible (details are in the Supplemental Information).

The results for the two different charge-state transitions, ox^0 and red^+, are displayed in Fig. 3 (the fitted Δf levels are shown in Figure S2). Fig. 3a,b show the evolution of $r(V_{probe})$ and their r_{sat} for the respective charge-state transition. In Fig. 3b a second z_{probe} demonstrates that r_{sat} can be tuned by z_{probe}. The tunneling rate Γ and single-electron tunnel current I for each transition are shown in Fig. 3c,d and are well described by an error function (indicated by a black line). The ox^0 and red^+ voltages (dashed red lines in Fig. 3c and d) are (-2.44 ± 0.04) V and (-1.48 ± 0.05) V, respectively. The errors stem mainly from the uncertainty of r in determining the saturation region r_{sat} (error analysis

is demonstrated in Figures S3–S5). The second z_{probe} measurement in Fig. 3b displayed a similar red^+ voltage level.

To obtain the ox^0 and red^+ energy levels from the corresponding voltages, the partial voltage drop across the NaCl dielectric film needs to be estimated. A calculation using a finite element model of the tip and the insulator provides a voltage drop of ≈ 17 % across the insulating film (see Figure S6 and [26]). Accordingly, this correction yields ox^0 and red^+ energy levels of (-2.04 $\pm$ 0.15) eV and (-1.23 $\pm$ 0.10) eV, respectively. The absolute difference between these two energies is E_{reorg}, quantified as (0.81 $\pm$ 0.18) eV for NPc on NaCl. The uncertainty in the reorganization energy value is comparable to the errors obtained from photoelectron spectroscopy on molecular films [27].

The full width at half maximum of the ox^0 and red^+ voltage levels were found to be distinctly different, being (0.6 $\pm$ 0.1) V and (0.25 $\pm$ 0.13) V, respectively. For an explanation of the difference in line widths, the potential energy landscape of NPc^0 and NPc^+ on NaCl along with the tip induced polarization of the film need to be addressed. This complex task deserves further investigation. The peak position of the ox^0 level can be compared to scanning tunneling spectroscopy measurements of NPc on bilayer NaCl [28]. The peak position for the bilayer (-1.7 V) is shifted upwards, the difference is discussed below. The peak width ($\approx$ 0.2 V) for the bilayer is smaller than the width reported here.

The measured values for the ox^0 and red^+ energy levels and the reorganization energy were corroborated by simulations based on density functional theory (DFT) of the film and the adsorbed molecule using a perfect conductor model of the metal support and a force field between the metal and the surface (see Methods for details). These energies were computed for NaCl thicknesses between 2 to 5 ML. Using finite-size scaling based on the asymptotic behaviour of these energies with the inverse number of NaCl monolayers N_l, the extrapolated values at 14 ML are -2.08 eV and -1.29 eV for the ox^0 and red^+ energy levels, respectively, and 0.79 eV for the hole reorganization energy (see Figure S7). These calculations are in good agreement with the corresponding experimental energies obtained above. However, the excellent agreement for the ox^0 and red^+ energy levels might be fortuitous because these energies involve a change of the charge state and, therefore, they are sensitive to the self-interaction error of the employed exchange-correlation functional in DFT. The measured upward shift of $\approx$ 0.3 eV of the ox^0 energy level for NPc on the bilayer NaCl compared to the 14 ML results is also in good agreement with the calculated value of 0.23 eV. This upward

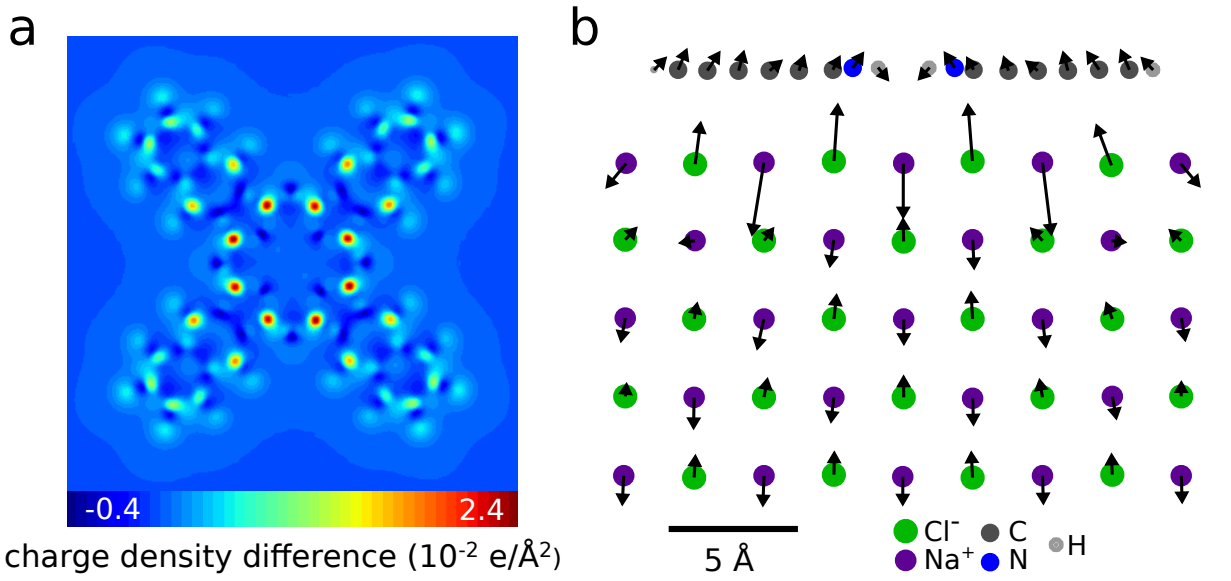

FIG. 4. DFT analysis of naphthalocyanine on NaCl(5 ML). **a,** 2D contour plot of the calculated charge density difference between $NPc^{+}_{geo^{+}}$ and $NPc^{0}_{geo^{+}}$ integrated outwards from the molecular plane to the vacuum region. **b,** Calculated atomic displacements of $NPc^{+}_{geo^{+}}$ with respect to $NPc^{0}_{geo^{0}}$. The map is the plane containing the non-polar direction of NaCl and along the center position of the imine nitrogens. The in-plane displacement vectors are magnified 40 times.

shift is predominantly caused by the image interaction with the metal surface (see Figure S7). At 14 ML, the calculated reorganization energy is dominated by the ionic polarization in the film. An extrapolation to $N_l = \infty$ increases the reorganization energy of NPc on 14 ML by only 0.06 eV. The intramolecular contribution to the hole reorganization energy is less than 3 %. A single image charge interaction model was used to estimate the influence of the metallic tip in the reorganization energy measurements. This estimate results in a small reduction of E_{reorg} of about 0.02 eV (see Figure S9).

The calculated charge density difference between $NPc^{+}_{geo^{+}}$ and $NPc^{0}_{geo^{+}}$ on NaCl(5 ML) is shown in Fig. 4a as a 2D contour plot of this density integrated outwards from the molecular plane to the vacuum region. This hole charge density is more or less delocalized over the molecule and is very similar to the corresponding density of NPc in the gas-phase (see Figure S8). This charge delocalization is consistent with the homogeneous ionic relaxation pattern of the 5 ML film upon charging which is shown in Fig. 4b. The major ionic response to the hole charge occurs in the NaCl surface layer, with the Na ions underneath the NPc

macrocycle having the greatest displacements ($\approx 7.5\,\mathrm{pm}$) reflecting a higher hole charge density in the macrocycle compared to the phenyl groups. The atoms in the subsurface layers show a similar displacement pattern but with significantly smaller displacements than for the surface layer. The similar magnitudes of these displacements in the subsurface layers are due to the long-range electric field from the delocalized hole charge density. Despite this charge delocalization, the relative large reorganization energy can be reconciled by the results of a simple dielectric model (details in the Supporting Information). Somewhat surprisingly, the molecule is displaced slightly upward ($\approx 2.0\,\mathrm{pm}$) upon charging.

In conclusion, we measured the hole reorganization energy caused by the charging of a single naphthalocyanine molecule adsorbed on top of an insulating NaCl film. Our method revolves around detecting single-electron transfer processes, based on the single-charge sensitivity of AFM that allows us to measure transition rates that corresponds to currents in the zeptoampere range. We corroborated and analyzed our results by density functional theory calculations, in which the metal support of the multilayer film is treated implicitly. The experimental method can be extended to other insulating films (ionic and non-ionic) as well as other adsorbates, different charge state transitions and be performed at elevated temperatures; moreover, it could also be applied to different AFM setups, provided conductive tips can be used. Quantification of the specific influence of the local environment on the reorganization energy of molecules and atoms on insulators can be readily achieved. The ability to measure reorganization energies at the atomic scale is indispensable to quantify and predict single electron transfer processes between molecules on insulating films and, in turn, tune and manipulate their energy transfer rates [29].

METHODS

STM and AFM measurements

Experiments were carried out with a combined scanning tunneling/atomic force microscope that utilizes a qPlus tuning fork sensor [30], which was operated in the frequency modulation mode [31] oscillating at 30.1 kHz. An oscillation amplitude of $A = 6\,\text{Å}$ was chosen to optimize the signal to noise ratio in detecting single charges. The microscope

was operated under ultrahigh vacuum ($p \approx 10^{-11}$ mbar) and low temperature ($T \approx 5$ K) conditions. The tip is made of PtIr and has been indented and characterized on the Cu(111) surface to yield and ensure a purely metallic tip, respectively. Voltages were applied to the sample. Positive height offsets used in z_{probe} refer to an increase in the tip–molecule distance. For the measurements in this letter, z_{set} was defined as the tip height of the imaging setpoint above the molecule (−1.7 Hz at 1 V). The z_{probe} was 10.2 Å from the imaging setpoint for probing the red^+ transition, corresponding to an effective tip–surface separation of about 22 Å (details are in the Supplemental Information). An increased z_{probe} of 11.2 Å was used for probing the ox^0 transition to ensure similar tunneling rates as measured for the red^+ transition while using lower V_{probe}.

Sample preparation

The substrate consisted of a 14 monolayer thick NaCl film grown on Cu(111) (for details on the thickness determination see Supplemental Material and [32]). This insulating layer prevents tunneling between NPc and the Cu(111). Evaporation of a low quantity of NPc molecules on top of the surface resulted in a low estimated coverage of ≈ 60 molecules per 1000×1000 $Å^2$ with molecules mostly being isolated from each other. Therefore, charge transfer between molecules was inhibited [33]. As noted in [28], no tautomerization of the molecule can be identified while detaching an electron from the HOMO of NPc.

DFT calculations

The ox^0 and red^+ energy levels and the hole reorganization energy of a single NPc molecule adsorbed on a NaCl film supported by a Cu(111) substrate were computed using a new method implemented in VASP [34] which allows charged systems outside a metal surface to be handled in a supercell geometry [35, 36]. In this method, the NaCl film and the adsorbed molecule were treated using DFT, whereas the support of the metals was described by a perfect conductor model and the residual interactions between the film and the metal were modelled by a simple force field. In this method the metal tip is not included.

In the calculations, the projector augmented wave (PAW) method [37] was used to describe the electron-ion interaction with a plane wave cut-off energy of 400 eV. The electronic exchange and correlation effects were treated using the optB86b version of the van der Waals (vdW) density functional [38–41]. The NaCl film was modelled by a slab with a [001] termination of bulk NaCl and 8×8 repetitions of the primitive surface unit cell, which corresponds to 64 Na and 64 Cl atoms in each layer. The film forms an incommensurate structure on the Cu(111) surface and as suggested by experiments for a bilayer [42], surface lattice constants of 3.895 Å, 3.91 Å, 3.93 Å and 3.94 Å were used in the calculations for the free-standing films with thicknesses between 2 to 5 ML, respectively. The same force field was used as for Cu(100), whereas the work function difference of 0.26 eV between NaCl films on Cu(100) and Cu(111), which only affects the transition energies, was accounted for by increasing the effective work function by the same amount. The cation was obtained by constraining the film and the molecule to have a net charge of $+1e$. The lateral electrostatic interactions between the periodic images were compensated by using a dipole-dipole correction scheme described in Ref. [43]. All atoms in the molecule and the NaCl film were allowed to relax during structural relaxations until the forces were less than 0.02 eV/Å. The Na site was found to be the most stable site of the adsorbed NPc molecule and the long axis of the molecule was oriented along $[1\bar{1}0]$ directions. The calculated adsorption energy of NPc on the NaCl trilayer is 5.04 eV, corresponding to about 60 meV per atom in accordance with the scaling of the physisorption interaction with molecular size [44]. The ox^0 and red^+ energy levels are given by the vertical transition energies,

$$\varepsilon_{\mathrm{ox}^0} = E(\mathrm{NPc}^0_{\mathrm{geo}^0}) - E(\mathrm{NPc}^+_{\mathrm{geo}^0}) \tag{2}$$

$$\varepsilon_{\mathrm{red}^+} = E(\mathrm{NPc}^0_{\mathrm{geo}^+}) - E(\mathrm{NPc}^+_{\mathrm{geo}^+}) \tag{3}$$

where the subscripts "geo^0" and "geo^+" refer to the equilibrium geometries of the neutral and positively charged systems, respectively. Note that in the calculation of the energy of NPc^+ the electron is detached to the Fermi level of the tip. The calculated reorganization energy λ is then simply given by,

$$\lambda = \varepsilon_{\mathrm{red}^+} - \varepsilon_{\mathrm{ox}^0}. \tag{4}$$

The data that support the results within this paper and other findings of this study are available from the corresponding author upon reasonable request.

* sfa at zurich.ibm.com

† Current address: Molecular Foundry, Lawrence Berkeley National Laboratory, California 94720, USA

‡ Current address: Daresbury Laboratory, Sc. Tech., Warrington, WA4 4AD, United Kingdom

[1] Joachim, C., Gimzewski, J. K. & Aviram, A. Electronics using hybrid-molecular and mono-molecular devices. *Nature* **408**, 541–548 (2000).

[2] Ratner, M. A brief history of molecular electronics. *Nat. Nanotech.* **8**, 378–381 (2013).

[3] Tao, N. J. Electron transport in molecular junctions. *Nat. Nanotech.* **1**, 173–181 (2006).

[4] Haiss, W. *et al.* Precision control of single-molecule electrical junctions. *Nat. Mater.* **5**, 995–1002 (2006).

[5] Moser, C. C., Keske, J. M., Warncke, K., Farid, R. S. & Dutton, P. L. Nature of biological electron transfer. *Nature* **355**, 796–802 (1992).

[6] Adams, D. M. *et al.* Charge Transfer on the Nanoscale: Current Status. *J. Phys. Chem. B* **107**, 6668–6697 (2003).

[7] Marcus, R. A. Electron transfer reactions in chemistry. Theory and experiment. *Rev. Mod. Phys.* **65**, 599–610 (1993).

[8] Vaissier, V., Barnes, P., Kirkpatrick, J. & Nelson, J. Influence of polar medium on the reorganization energy of charge transfer between dyes in a dye sensitized film. *Phys. Chem. Chem. Phys.* **15**, 4804–4814 (2013).

[9] Brunschwig, B. S., Ehrenson, S. & Sutin, N. Solvent reorganization in optical and thermal electron-transfer processes. *J. Phys. Chem.* **90**, 3657–3668 (1986).

[10] Repp, J., Meyer, G., Paavilainen, S., Olsson, F. E. & Persson, M. Scanning Tunneling Spectroscopy of Cl Vacancies in NaCl Films: Strong Electron-Phonon Coupling in Double-Barrier Tunneling Junctions. *Phys. Rev. Lett.* **95**, 225503 (2005).

[11] Manke, F., Frost, J. M., Vaissier, V., Nelson, J. & Barnes, P. R. F. Influence of a nearby substrate on the reorganization energy of hole exchange between dye molecules. *Phys. Chem. Chem. Phys.* **17**, 7345–7354 (2015).

[12] Moth-Poulsen, K. & Bjørnholm, T. Molecular electronics with single molecules in solid-state devices. *Nat. Nanotech.* **4**, 551–556 (2009).

[13] Eckermann, A. L., Feld, D. J., Shaw, J. A. & Meade, T. J. Electrochemistry of redox-active self-assembled monolayers. *Coord. Chem. Rev.* **254**, 1769–1802 (2010).

[14] Blackbourn, R. L. & Hupp, J. T. Probing the molecular basis of solvent reorganization in electron-transfer reactions. *J. Phys. Chem.* **92**, 2817–2820 (1988).

[15] Bredas, J. L. & Street, G. B. Polarons, bipolarons, and solitons in conducting polymers. *Acc. Chem. Res.* **18**, 309–315 (1985).

[16] Gruhn, N. E. *et al.* The Vibrational Reorganization Energy in Pentacene: Molecular Influences on Charge Transport. *J. Am. Chem. Soc.* **124**, 7918–7919 (2002).

[17] Duhm, S. *et al.* Charge Reorganization Energy and Small Polaron Binding Energy of Rubrene Thin Films by Ultraviolet Photoelectron Spectroscopy. *Adv. Mater.* **24**, 901–905 (2012).

[18] Stomp, R. *et al.* Detection of Single-Electron Charging in an Individual InAs Quantum Dot by Noncontact Atomic-Force Microscopy. *Phys. Rev. Lett.* **94**, 056802 (2005).

[19] Bussmann, E. & Williams, C. C. Single-electron tunneling force spectroscopy of an individual electronic state in a nonconducting surface. *Appl. Phys. Lett.* **88**, 263108 (2006).

[20] Gross, L. *et al.* Measuring the Charge State of an Adatom with Noncontact Atomic Force Microscopy. *Science* **324**, 1428–1431 (2009).

[21] Roy-Gobeil, A., Miyahara, Y. & Grutter, P. Revealing Energy Level Structure of Individual Quantum Dots by Tunneling Rate Measured by Single-Electron Sensitive Electrostatic Force Spectroscopy. *Nano Lett.* **15**, 2324–2328 (2015).

[22] Miyahara, Y., Roy-Gobeil, A. & Grutter, P. Quantum state readout of individual quantum dots by electrostatic force detection. *Nanotechnology* **28**, 064001 (2017).

[23] Bevan, K. H. Electron transfer from the perspective of electron transmission: Biased non-adiabatic intermolecular reactions in the single-particle picture. *J. Chem. Phys.* **146**, 134106 (2017).

[24] Jortner, J. Temperature dependent activation energy for electron transfer between biological molecules. *J. Chem. Phys.* **64**, 4860–4867 (1976).

[25] Repp, J., Meyer, G., Stojković, S. M., Gourdon, A. & Joachim, C. Molecules on Insulating Films: Scanning-Tunneling Microscopy Imaging of Individual Molecular Orbitals. *Phys. Rev. Lett.* **94**, 026803 (2005).

[26] Feenstra, R. M. Electrostatic potential for a hyperbolic probe tip near a semiconductor. *J. Vac. Sci. Technol. B* **21**, 2080 (2003).

[27] Kera, S. & Ueno, N. Photoelectron spectroscopy on the charge reorganization energy and small polaron binding energy of molecular film. *J. Electron. Spectrosc. Relat. Phenom.* **204**, 2–11 (2015).

[28] Liljeroth, P., Repp, J. & Meyer, G. Current-Induced Hydrogen Tautomerization and Conductance Switching of Naphthalocyanine Molecules. *Science* **317**, 1203–1206 (2007).

[29] Imada, H. *et al.* Real-space investigation of energy transfer in heterogeneous molecular dimers. *Nature* **538**, 364–367 (2016).

[30] Giessibl, F. J. High-speed force sensor for force microscopy and profilometry utilizing a quartz tuning fork. *Appl. Phys. Lett.* **73**, 3956 (1998).

[31] Albrecht, T. R., Grutter, P., Horne, D. & Rugar, D. Frequency modulation detection using high-Q cantilevers for enhanced force microscope sensitivity. *J. Appl. Phys.* **69**, 668 (1991).

[32] Steurer, W., Gross, L. & Meyer, G. Local thickness determination of thin insulator films via localized states. *Appl. Phys. Lett.* **104**, 231606 (2014).

[33] Steurer, W., Fatayer, S., Gross, L. & Meyer, G. Probe-based measurement of lateral single-electron transfer between individual molecules. *Nat. Commun.* **6**, 8353 (2015).

[34] Kresse, G. & Joubert, D. From ultrasoft pseudopotentials to the projector augmented-wave method. *Phys. Rev. B* **59**, 1758–1775 (1999).

[35] Scivetti, I. & Persson, M. The electrostatic interaction of an external charged system with a metal surface: a simplified density functional theory approach. *J. Phys.: Condens. Matter* **25**, 355006 (2013).

[36] Scivetti, I. & Persson, M. A simplified density functional theory method for investigating charged adsorbates on an ultrathin, insulating film supported by a metal substrate. *J. Phys.: Condens. Matter* **26**, 135003 (2014).

[37] Blöchl, P. E. Projector augmented-wave method. *Phys. Rev. B* **50**, 17953–17979 (1994).

[38] Klimeš, J., Bowler, D. R. & Michaelides, A. Van der Waals density functionals applied to solids. *Phys. Rev. B* **83**, 195131 (2011).

[39] Dion, M., Rydberg, H., Schröder, E., Langreth, D. C. & Lundqvist, B. I. Van der Waals Density Functional for General Geometries. *Phys. Rev. Lett.* **92**, 246401 (2004).

[40] Thonhauser, T. *et al.* Van der Waals density functional: Self-consistent potential and the nature of the van der Waals bond. *Phys. Rev. B* **76**, 125112 (2007).

[41] Román-Pérez, G. & Soler, J. M. Efficient Implementation of a van der Waals Density Func-

tional: Application to Double-Wall Carbon Nanotubes. *Phys. Rev. Lett.* **103**, 096102 (2009).

[42] Repp, J. *et al.* Charge-State-Dependent Diffusion of Individual Gold Adatoms on Ionic Thin NaCl Films. *Phys. Rev. Lett.* **117**, 146102 (2016).

[43] Scivetti, I. & Persson, M. Frontier molecular orbitals of a single molecule adsorbed on thin insulating films supported by a metal substrate: electron and hole attachment energies. *J. Phys.: Condens. Matter* **29**, 355002 (2017).

[44] Björk, J. *et al.* Adsorption of Aromatic and Anti-Aromatic Systems on Graphene through π-π Stacking. *J. Phys. Chem. Lett.* **1**, 3407–3412 (2010).

ACKNOWLEDGMENTS

We thank Rolf Allenspach for comments. Financial support by the European Research Council (Advanced grant 'CEMAS' - agreement no. 291194 and Consolidator grant 'AMSEL' - agreement no. 682144), EU projects 'PAMS' (Contract. No. 610446) and Initial Training Network 'ACRITAS' (Contract No. 317348). The Leverhulme Trust (F/00 025/AQ) and the allocations of computer resources at Chadwick, The University of Liverpool are gratefully acknowledged. I.S. acknowledges CCP5 funding and associated CoSeC support at STFC via EPSRC grant no. EP/M022617/1 and SLA for funding.

AUTHOR CONTRIBUTIONS

S.F, W.S, J.R, L.G. and G.M designed the experiments. S.F., B.S., L.G. and G.M. performed the experiments. S.F. carried out the finite element simulations. M.P. and I.S. were responsible for the DFT calculations. All authors discussed the results and wrote the manuscript.

COMPETING INTERESTS

The authors declare no competing financial interests.

ADDITIONAL INFORMATION

Supplementary information is available in the online version of the paper.
Reprints and permission information is available online at www.nature.com/reprints.
Correspondence and requests for materials should be addressed to S.F.